Combinatorial Synthesis and Evaluation of Functional Inorganic Materials Using Thin-Film Techniques

Ichiro Takeuchi, Robert Bruce van Dover, and Hideomi Koinuma

Abstract

Novel phases of functional inorganic chemical systems can be efficiently explored using high-throughput thin-film fabrication techniques coupled with rapid characterization schemes. High-throughput investigation of thin-film materials has already led to the discovery of new dielectric and magnetic materials. In this article, we review various high-throughput thin-film synthesis/evaluation techniques and discuss examples of exciting discoveries and new applications of combinatorial techniques.

Keywords: *advanced dielectrics, combinatorial methods, composition spreads, concurrent x-ray diffractometer, thin films, laser molecular-beam epitaxy, scanning evanescent microwave probe, transparent magnetic materials.*

Introduction

The discovery of novel functional materials can be efficiently accomplished using high-throughput thin-film fabrication techniques coupled with rapid characterization schemes. Combinatorial thin-film "libraries" have been prepared using discrete, sequentially masked depositions, codeposited composition spreads, and composition-gradient molecular layer epitaxy. Measurement techniques have been adapted for quick evaluation of the libraries and composition spreads, mapping a variety of physical characteristics including optical, electrical, and magnetic properties. High-throughput investigation of thin-film materials has already led to the discovery of exciting new and useful dielectric ($Zr_{0.2}Sn_{0.2}Ti_{0.6}O_2$; $Ba_{0.12-0.25}Sr_{0.35-0.47}Ca_{0.32-0.53}TiO_3$) and magnetic (Co-doped TiO_2) materials. It has also facilitated investigations of the detailed composition dependence of properties in systems that are already known but have been incompletely studied. In this article, we review successful discoveries and applications of these combinatorial materials libraries.

Thin-Film Library Synthesis

The effort to directly transfer the organic combinatorial synthesis concept to inorganic thin-film materials was started by a group at the Lawrence Berkeley National Laboratory.[1] In adopting this synthetic approach to simultaneously creating large arrays of thin-film samples, the precursor deposition method was used. This approach can truly bring out the combinatorial nature of the synthesis because it enables the production of a large number of different compositions by generating many permutations of precursors. On a substrate as small as 1 cm^2, thousands of different compositions can be integrated, synthesized, and screened for desired physical properties in a single experiment. This method takes advantage of the fact that in many materials systems it is possible to grow stoichiometric compounds by means of controlled thermal diffusion of precursors. For fabricating $YBa_2Cu_3O_7$, for instance, one can use amorphous layers of Y_2O_3, BaF_2, and CuO_2 as precursors. A series of precisely positioned shadow masks, which allow spatially selective depositions, are used to deposit different combinations of precursors at different positions on a substrate at room temperature in order to generate diverse compositional variation across a library. For instance, in the quaternary combinatorial masking scheme (shown in Figure 1), each mask is used in up to four depositions on a square substrate of the same size with four different orientations (rotated 90° from each other). After the first mask is used, four quadrants have four different materials deposited through the open windows. Going from one mask to the next, the regions of openings (windows) continue to be subdivided into further quadrants. In this way, using n masks, after carrying out $4 \times n$ depositions, 4^n *discrete* combinations of precursors can be created on a given chip. Sputtering, evaporation, and pulsed laser deposition are some of the physical vapor deposition techniques that have proven to be useful for precursor deposition. Following the deposition step, libraries undergo controlled thermal treatments to (1) diffuse and mix the precursors and (2) crystallize compounds (if desired) at each site.

The utility and effectiveness of combinatorial synthesis using the precursor method was first demonstrated with high-T_c superconductors.[1] Soon after this first proof of principle, a combinatorial library was used to identify a class of cobalt oxide magnetoresistive materials of the form $(La_{1-x}Sr_x)CoO_3$.[2]

Because the formation of phases through postannealing relies largely on thermodynamic equilibrium, the precursor method cannot be considered a universal solution. The success and integrity of this method depend on how well one can map the trend

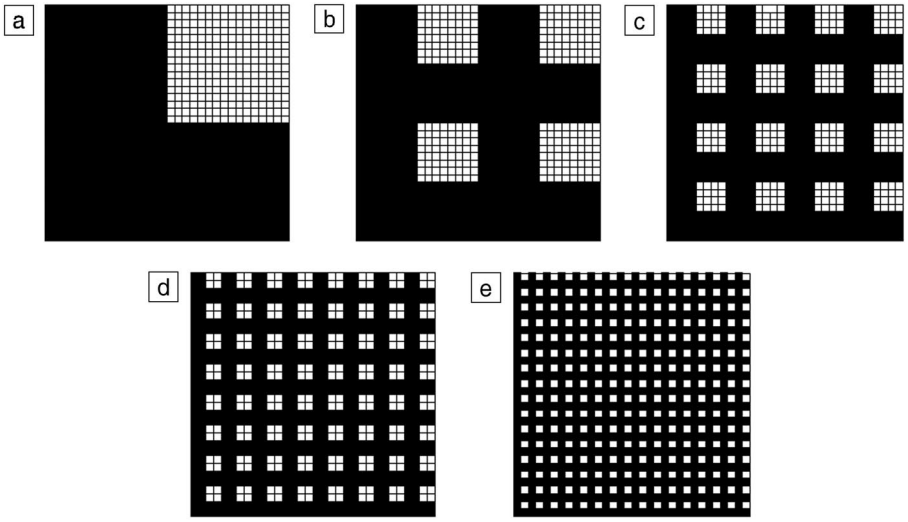

Figure 1. (a)–(e) Shadow mask patterns used for quaternary design of combinatorial libraries. Each mask is used in up to four depositions on a square substrate of the same size with four different orientations rotated 90° from each other. After the first mask is used, four quadrants have four different materials deposited through the open windows. Moving from one mask to the next, the regions of openings (windows) continue to be subdivided into further quadrants. In this way, using n *masks, after carrying out* $4 \times$ n *depositions,* 4^n *discrete combinations of precursors can be created on a given chip.*

with which the compositional variation changes the physical properties across the library. Applicability of the precursor method to a specific materials system needs to be determined on a case-by-case basis, and it depends on the degree to which defects affect the macroscopic physical property of interest.

This method has been demonstrated to produce predominantly single-phase epitaxial films on lattice-matched substrates as determined by x-ray diffraction.[3–5] High-resolution cross-sectional transmission electron microscopy (TEM) studies have been performed on $Ba_{1-x}Sr_xTiO_3$ films made from BaF_2, SrF_2, and TiO_2 precursors.[6] They reveal that the resulting films do indeed consist of epitaxial grains with atomically sharp interfaces with the (100) $LaAlO_3$ substrate.

Codeposition from two or more spatially separated sources can be used to obtain samples with a natural composition gradient. The crucial advantage of codeposition is that the material is intimately mixed in the as-deposited state, so it is possible to prepare metastable and low-temperature phases that are not accessible by any other route. Codeposition schemes can be problematic, as the composition is not directly controlled and compositions must be inferred indirectly. However, it is generally possible to model the position dependence of the deposition rate from the various sources, and compositions accurate to ~5 at.% can be calculated. Energy-dispersive spectroscopy, wavelength-dispersive spectroscopy, and Rutherford backscattering spectroscopy are some of the techniques used for obtaining compositional mapping.

In view of the fact that every crystalline material is composed of molecular layers stacked periodically and that modern electronic devices have nanoscale layer structures,[7] it is desirable to develop a scheme for the parallel fabrication of layered structures so that we can quickly find the best matching of layered lattices and optimum fabrication conditions. The Koinuma group implemented the methods of combinatorial laser molecular-beam epitaxy (CLMBE)[8,9] to create artificial oxide lattices and heterojunctions, with each layer composition, thickness, and sequence controlled at the atomic scale. Molecular layers are deposited from several kinds of solid sources through a series of physical shadow masks placed on a heated substrate, and the deposited materials are crystallized in as-grown states.

The effectiveness of combinatorial lattice integration using the CLMBE system was demonstrated in the concurrent fabrication of a set of $SrTiO_3/BaTiO_3$ (STO/BTO) superlattices with equimolar ratios and different periodicities at an oxygen pressure of 1.0×10^{-6} Torr and a substrate temperature of 700°C.[10,11] The use of chemically etched $SrTiO_3$(001) substrates with atomically flat surfaces enabled observation of clear reflection high-energy electron diffraction (RHEED) intensity oscillations, each of which corresponded to the growth of a unit-cell layer (0.4 nm) of each oxide. Synchronization of the RHEED beam sweeping across the substrate surface with a pair of coils and image acquisition were combined with moving physical masks to simultaneously control the growth of as many as 10 stripe-patterned thin films in parallel on a single substrate. RHEED traces for the growth of three different periodicities are shown in Figure 2. Incorporating 90° substrate rotation can enable fabrication of as large as a 10×10 matrix of superlattices.

Rapid Screening of Physical Properties

The scope of the materials systems and properties that can be addressed is often constrained by the availability and capabilities of high-throughput characterization techniques. These include parallel measurement/detection systems or various scanning probe microscopes, depending on the specific physical property of interest. Many well-established technologies can be used to map compositions and physical properties. Here we discuss two innovative technologies.

The scanning evanescent microwave microscope has proven to be a powerful characterization tool that can provide quantitative electrical-impedance mapping of a variety of thin-film libraries.[3,4,12–15] It consists of a $\lambda/4$ (quarter-wave) Cu coaxial resonator with a tapered center conductor. A sharp metal tip mounted on the center conductor extends beyond an aperture in the center of the end wall (Figure 3). As the resonator-tip assembly is scanned over a sample surface, changes in the resonant frequency f and the quality factor Q (the ratio of the energy-storing capability to energy-dissipating capability) of the resonator caused by the electromagnetic near-field interaction of the tip with the local sample surface are recorded to obtain images. Using a quasi-static electric-field-distribution calculation, changes in f and Q can be directly converted to real and imaginary parts of the complex dielectric constant.[13] With its ability to nondestructively measure dielectric constant and sheet resistance, the microscope has been used for studying ferroelectric/dielectric materials in general and superconductors.[14] Variable temperature and multifrequency measurement features can be added to expand the capabilities and the scope of investigation using the microscope.[15]

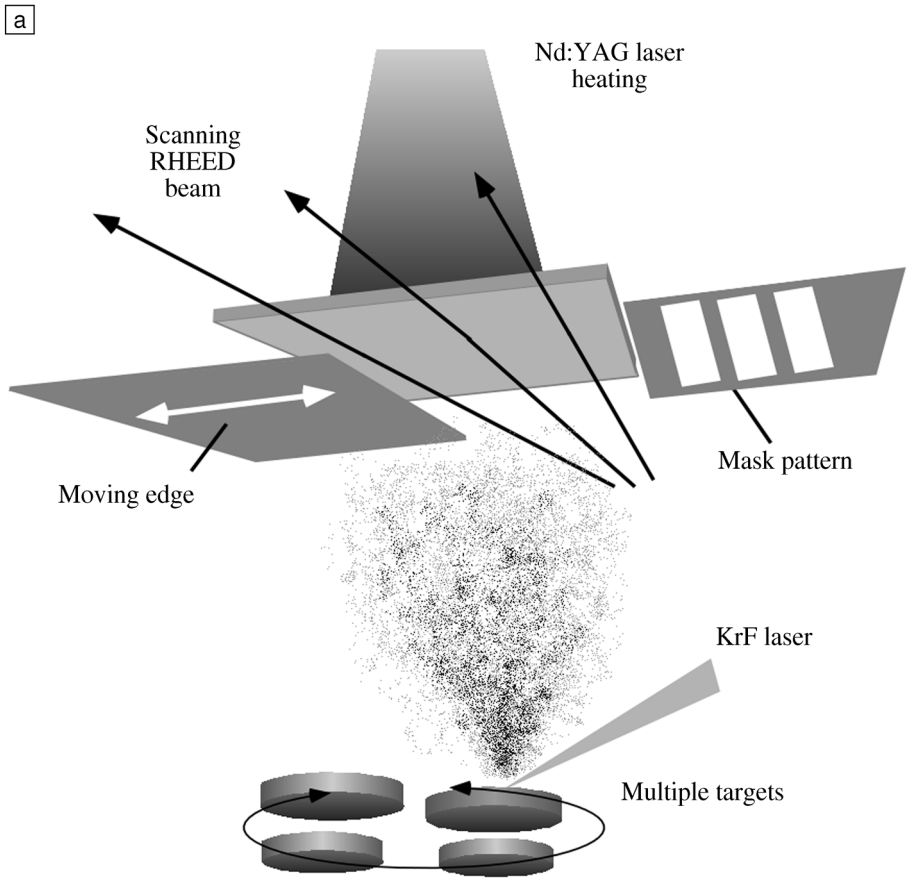

Figure 2. Fabrication of an atomically controlled materials library. (a) Schematic setup for parallel growth of epitaxial superlattices. (b) Simultaneously obtained reflection high-energy electron diffraction (RHEED) intensities versus time for three $SrTiO_3/BaTiO_3$ superlattices fabricated on a single atomically controlled materials library chip. The deposition sequence is shown below the graph.

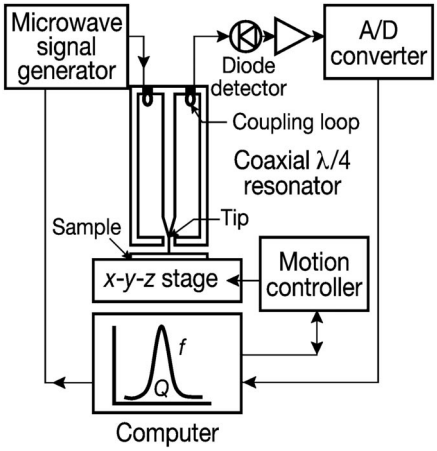

Figure 3. Schematic illustration of a scanning evanescent microwave microscope consisting of a Cu coaxial resonator with a tapered center conductor. A sharp metal tip mounted on the center conductor extends beyond an aperture in the center of the end wall. As the resonator-tip assembly is scanned over a sample surface, changes in the resonant frequency f *and the quality factor* Q *of the resonator caused by the electromagnetic near-field interaction of the tip with the local sample surface are recorded to obtain images.*

Structural characterization of libraries and spreads by x-ray diffraction is an important part of combinatorial experiments. One way to perform rapid x-ray characterization is to use a focused synchrotron x-ray microbeam. This has been successfully used for rapid phase mapping and composition mapping (using fluorescence) of combinatorial libraries.[16,17] For in-house applications, a concurrent x-ray diffractometer has been developed,[18] which consists of a convergent x-ray beam source ($Cu\ K_{\alpha 1}$) with a dispersion of 2° formed by a rotating anode x-ray source and proper x-ray optics (including a cylindrical, Johann-type mirror for converging x-rays), a conventional powder diffraction goniometer, and a two-dimensional detector (imaging plate or charge-coupled device, Figure 4a).

Figures 4b and 4c are from a concurrent x-ray diffractometer measurement, where the beam was focused into a 10 mm × 1 mm line on an integrated superlattice chip to generate a two-dimensional-intensity image on the detector. On this chip, there were 10 superlattices: $[(SrTiO_3)_m/(BaTiO_3)_n]_{30}$ ($m = n = 12, 14, 16, \ldots, 28$, and 30) (Figure 4d). In addition to the specularly reflected band near 0.70° and the reflected $SrTiO_3(001)$ band near 22.75°, one clearly observes reflection lines at the angles

corresponding to the designed periodicities of the individual superlattices. The line profiles extracted from the $[(SrTiO_3)_{12}/(BaTiO_3)_{12}]_{30}$ diffraction patterns are also shown in Figures 4e and 4f.

A similar microdiffractometer with a point x-ray source (diameter of down to 50 μm) has also been used in two-dimensional phase mapping of libraries and spreads.[15]

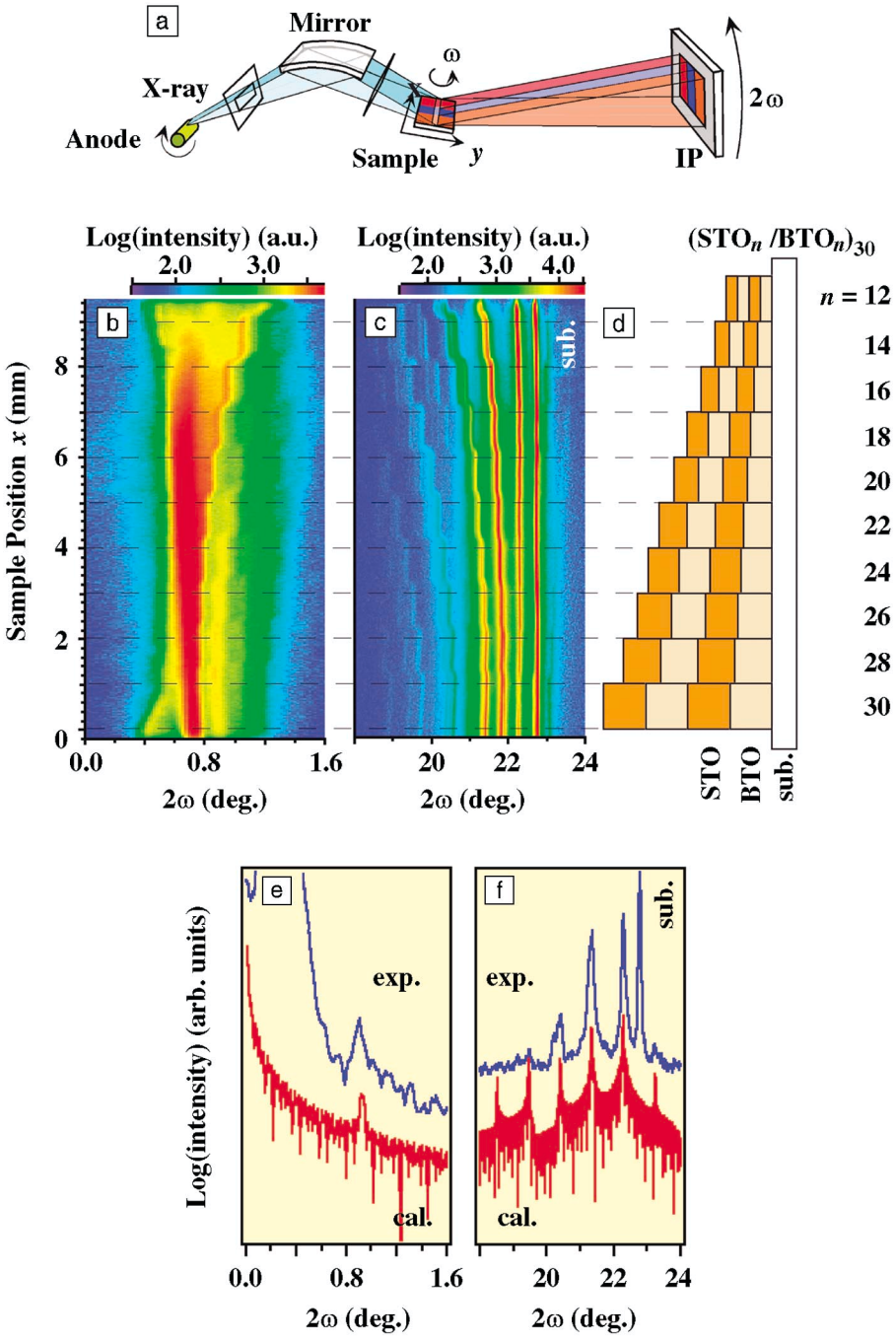

Figure 4. Characterization of atomically controlled combinatorial libraries using a concurrent x-ray diffractometer. (a) Schematic illustration of the setup. (b), (c) Concurrent x-ray diffraction data from a $[(BaTiO_3)_m/(SrTiO_3)_n]$ superlattice library for two ranges of 2ω. (d) Cross-sectional diagram of the superlattices. On this chip, there were 10 superlattices: $[(SrTiO_3)_n/(BaTiO_3)_n]_{30}$ (n = 12, 14, 16, . . . , 28, and 30). (e), (f) Line profiles extracted from the diffraction patterns of $[(SrTiO_3)_{12}/(BaTiO_3)_{12}]_{30}$.

New Compositions of Ferroelectric and Dielectric Materials

Thin films of $(Ba,Sr)TiO_3$ are widely pursued for embedded dynamic random-access memory (DRAM) capacitors as well as for various tunable microwave device applications. The precursor method using the quaternary masking scheme was successfully implemented for fabricating libraries with discrete patterns for systematic doping studies into $(Ba,Sr)TiO_3$; W was identified as a metallic dopant that helps reduce the dielectric loss at microwave frequencies.[3] Compared with undoped $BaTiO_3$, W doping decreases microwave loss by a factor of ~4 at 1 GHz. The effect of W doping has since been confirmed by other groups who have fabricated doped $(Ba,Sr)TiO_3$ films using conventional thin-film deposition techniques.[19] In a related study, capacitor device libraries incorporating all epitaxial multilayer structures into a compositionally varying background were fabricated, and W doping was also found to reduce the dc leakage current in capacitors.[5] It is believed that a small trace of W (up to ~2 mol%) introduced in the host substitutes on the Ti site and reduces the quantity of oxygen vacancies formed in the crystallization process of $(Ba,Sr)TiO_3$, thus reducing the overall loss of the compound.

An automated gliding shutter was used to make a continuous compositional spread fabricated from precursors, where the $(Ba,Sr,Ca)TiO_3$ ternary system was mapped on a triangular chip of $LaAlO_3(100)$ (Figure 5).[4] In order to lay out the ternary phase diagram, three gradient depositions were performed in three different directions for three precursors, $BaCO_3$, $CaCO_3$, and $SrCO_3$. A large fraction of this phase diagram had never been produced in either bulk or thin films prior to this study. The images shown in Figure 5 are dielectric-constant images obtained as a result of scanning evanescent microwave microscopy performed on the chip. Figure 5a is an ε plot, and Figure 5b is a tan δ plot. From this study, a new low-microwave-loss region, $Ba_{0.12-0.25}Sr_{0.35-0.47}Ca_{0.32-0.53}TiO_3$, was successfully identified without compromising the value of ε.

A recent codeposition study[20] employed three magnetron sputtering guns in the 90° off-axis configuration to form a two-dimensional pseudoternary spread of oxide dielectric materials (Figure 6). Over 30 chemical systems were explored in this study, resulting in the identification of amorphous $Zr_{0.2}Sn_{0.2}Ti_{0.6}O_2$ as a particularly promising material. For each chemical system, a codeposited composition spread was prepared on a 7 cm × 7 cm

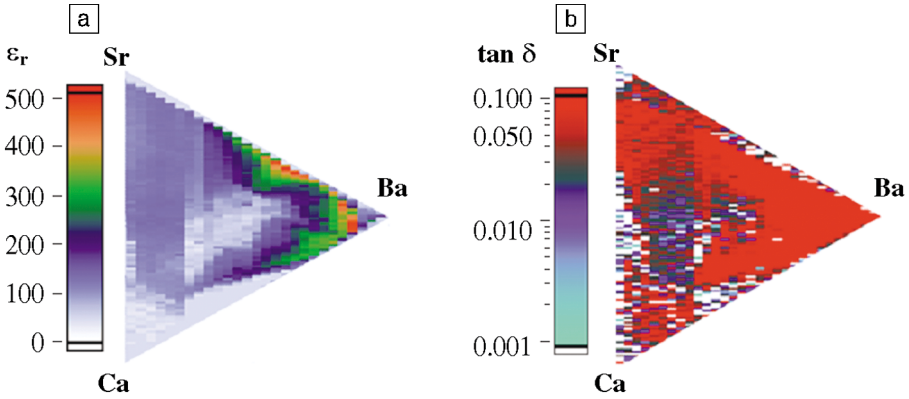

Figure 5. Scanned images of a (Ba,Sr,Ca)TiO_3 composition spread fabricated on a triangular $LaAlO_3$ substrate. (a) An ε plot (ε_r is the relative dielectric constant), and (b) a tan δ plot (ratio between the imaginary and the real part of the dielectric constant), both obtained with the scanning evanescent microwave microscope. A new low-microwave-loss region, $Ba_{0.12-0.25}Sr_{0.35-0.47}Ca_{0.32-0.53}TiO_3$, was identified. (From Reference 4.)

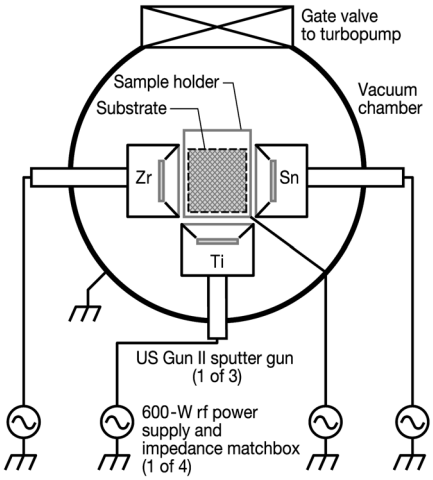

Figure 6. Schematic diagram of an off-axis sputtering system used for the preparation of two-dimensional pseudoternary oxide dielectrics.

substrate coated with a metallic base electrode. The deposition was performed using metal targets and a reactive Ar-O_2 atmosphere. The capacitance and current–voltage characteristics of the resulting films were measured using a scanning Hg probe counter electrode, and a virtual array of about 4000 measurements was constructed by making measurements of the film on 1-mm centers. The product of the capacitance and breakdown voltage, normalized to the area of the Hg counter electrode, is an important figure of merit for capacitor materials, as it represents the maximum charge per unit area that can be stored in the capacitor. This product is plotted in Figure 7a for a sample made in the Zr-Sn-Ti-O system, and the data are replotted in a standard ternary chart in Figure 7b. It is immediately obvious that compositions in the vicinity of $Zr_{0.2}Sn_{0.2}Ti_{0.6}O_2$ have optimal properties, with a maximum stored charge of about 25 $\mu C/cm^2$. This value compares favorably with the value obtained for deposited films of SiO_2 (3–5 $\mu C/cm^2$), Al_2O_3 (6–10 $\mu C/cm^2$), and Ta_2O_5 (10–12 $\mu C/cm^2$). Films made by conventional single-composition on-axis sputtering were subsequently shown to yield identical results,[21] raising the prospect that this material might prove useful as an alternative dielectric for DRAM capacitors, although the superior properties have not yet been demonstrated in films synthesized by chemical vapor deposition, the synthetic technique of choice in the Si integrated-circuit industry.

Automated evaluation techniques can also improve the throughput of studies of the composition dependence of materials properties. Here the fine granularity with which we can delineate the composition dependence can sometimes provide unique insights. For example, in the van Dover group, the behavior of the dielectric constant in the pseudobinary system Zr-Al-O,[22] a system that might prove useful as an alternative gate dielectric for advanced Si integrated circuits, was studied.[23] For this application, a dielectric is sought that is amorphous, thermodynamically stable in contact with Si,[24] and has a dielectric constant of $12 < \varepsilon < 50$, among other criteria. Compositions in the Zr-Al-O system are expected to meet these criteria. One might expect that the dielectric constant would be a slowly varying function of composition in an amorphous system, so when the composition dependence of the dielectric constant was evaluated (Figure 8), the

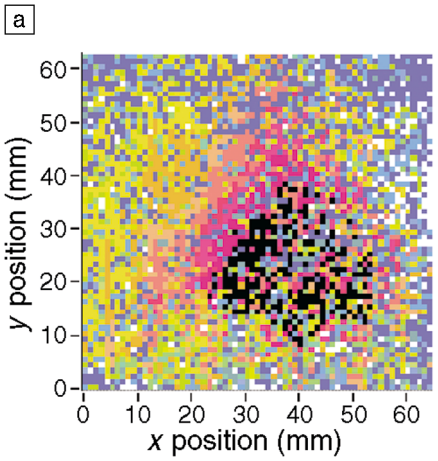

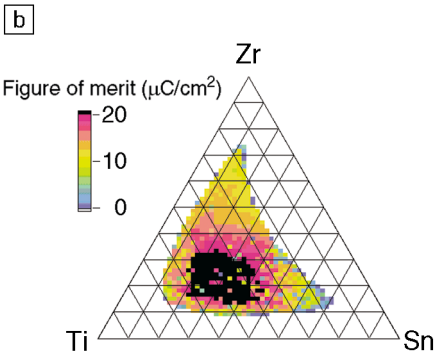

Figure 7. (a) Figure of merit (maximum stored charge per unit area, obtained from the product of capacitance and breakdown voltage, normalized to capacitor area) for an amorphous Zr-Sn-Ti-O composition spread. (b) Data in (a) plotted as a function of composition in a conventional ternary plot. The experiment, from chamber pumpdown to printout of the ternary diagram, was completed in under 24 h. (From Reference 20.)

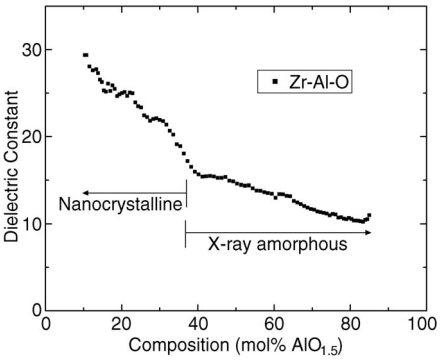

Figure 8. Dielectric constant as a function of composition in the Zr-Al-O system proposed as an alternative gate dielectric in advanced field-effect transistors.

results were surprising. The dense data clearly delineate an abrupt transition in the dielectric constant. Subsequent evaluation of the composition spread using high-sensitivity x-ray diffraction verified the hypothesis that the ZrO_2-rich compositions, with their high dielectric constant, were in fact nanocrystalline. Less dense coverage of the composition dependence might have missed the transition in ε and therefore would not have motivated the careful x-ray study.

Intematix Corp. recently applied the combinatorial thin-film library technique to discover advanced microwave tunable dielectrics, as discussed in the accompanying sidebar article.

Discovery of Optically Transparent Ferromagnets

Another good example of serendipitous discovery brought about by the combinatorial approach is the unexpected finding of optically transparent magnetism in TiO_2 anatase films doped with Co.[25] Ferromagnetic semiconductors formed by doping magnetic impurities into host semiconductors are key materials for spin electronics, where the correlation between the spin and the charge of electrons gives rise to spin-dependent functionalities such as giant magnetoresistance and spin field-effect transistors. All known magnetic semiconductors until now had been based on nonoxides such as GaAs and ZnSe, and their highest Curie temperature was ~100 K. There was a theoretical prediction that ZnO would become ferromagnetic when doped with certain 3*d* transition elements, but to date no sign of ferromagnetism has been observed in such systems.

Titanium dioxide (TiO_2) is commonly used for photocatalysis for water cleavage and is well known for its unique properties including high refractive index, excellent optical transmittance in the visible and infrared regions, and high dielectric constant. Libraries of 3*d* transition-metal-doped TiO_2 were originally fabricated by CLMBE in a search for photocatalysts. When their magnetic properties were

Combinatorial Synthesis of Advanced Microwave Tunable Dielectrics

Yi-Qun Li

A combinatorial materials science approach was recently applied by the Intematix Corp. of Moraga, Calif., to optimize a tunable barium strontium titanate system with the objective of lowering its dielectric loss (tan δ_ε) while retaining its high dielectric tunability. $(Ba_{0.6}Sr_{0.4})TiO_3$ (BST) was systematically studied with transition-metal ions M as substitutions for Ti. The generic formula is $(Ba_{0.6}Sr_{0.4})Ti_{1-x}M_xO_3$. A 1-in.^{2} $LaAlO_3$ substrate was used, and three libraries of $(Ba_{0.6}Sr_{0.4})(Ti_{1-x}M_x)O_3$ with M = A and B, and x continuously changing from 0 to 0.3, were synthesized by the combinatorial ion-beam deposition process.

A recently developed microbeam x-ray diffractometer/x-ray fluorescence spectrometer with a beam size of 50 μm (beam sizes from 20 μm to 100 μm can be selected) and sample scanning capability was used for the high-throughput screening of material composition and crystal structures. Figure 1 shows an x-ray diffraction (002) profile as a function of composition for BST-A and BST-B libraries. It is clearly observed in Figure 1a that the lattice constant of the highly oriented BST-A library film decreases (diffraction angle increases) with A concentration,

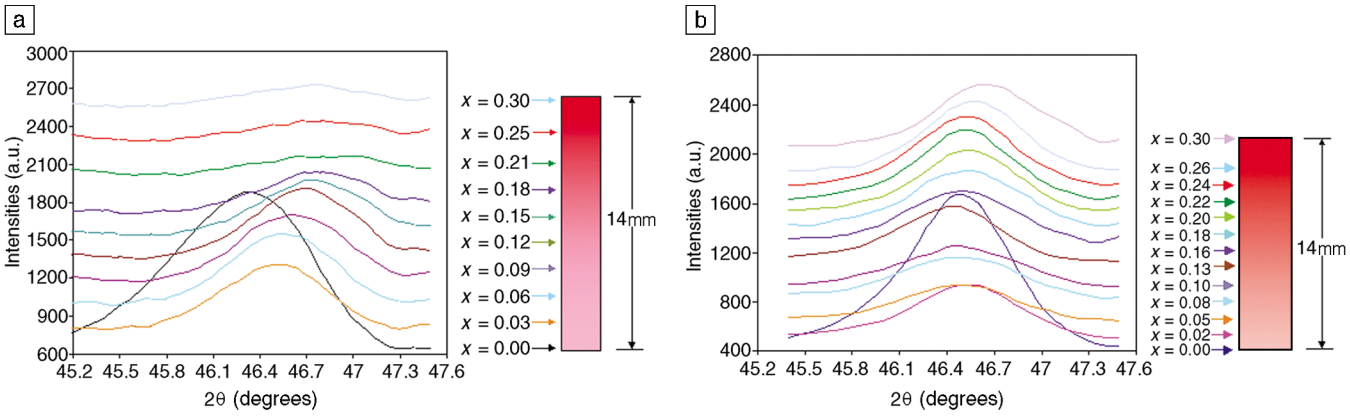

Figure 1. X-ray diffraction (002) profile as a function of composition for (a) BST-A (0–30%) and (b) BST-B (0–30%) libraries, which are synthesized by ion-beam sputtering and postannealing on single-crystal $LaAlO_3$ substrates with linear composition x ranging from 0% to 30% for M.

checked with a scanning superconducting quantum interference device (SQUID) microscope, Co-doped TiO_2 was found, surprisingly, to exhibit ferromagnetism at room temperature while maintaining its transparency and single phase up to a composition of 8% Co. In order to systematically study the changes of film properties as a function of doping level, a library containing nine $Ti_{1-x}Co_xO_2$ films with different x values was fabricated. TEM of the films has indicated no sign of segregation of impurity phases in the Co/Ti compositional range of $x < 0.08$.

Figure 9 shows a series of images taken with the SQUID microscope at 3 K for anatase films with different Co contents ($x = 0$–0.06) on a combinatorial chip. In all of the Co-doped films, magnetic-domain structures of around 20 μm are observed. With increasing Co content in the film, the magnitude of the magnetic field is systematically enhanced as a result of increased spontaneous magnetization. This observation established the presence of long-range order in the Co-doped TiO_2 anatase phase. Further magnetic characterization indicated that the films are ferromagnetic even at room temperature. The spontaneous magnetic moment per Co atom was deduced to be 0.32 μ_B from M–H curves. From a temperature-dependent magnetization measurement, T_c was estimated to be higher than 400 K, significantly higher than that for known nonoxide ferromagnetic semiconductors. At present, the exact nature of the magnetic long-range order in Co-doped TiO_2 is not understood. Recently, Co-doped TiO_2 rutile films were also found to exhibit robust ferromagnetism at room temperature.[26] The films were also found to display excellent optical transmission with a bandgap of 400 nm (3.1 eV). Transparent ferromagnets have a large potential for serving the integration of electronic circuits and magnetic storage with the user interface in a single flat-panel display.

Acknowledgments

We are grateful to many colleagues for extensive collaboration and many insightful

and the solubility of A in the BST phase is about 18%. Figure 1b shows a high solubility of B in BST of up to 30% with little change in lattice parameter as B concentration increases.

Dielectric characterization of the libraries was carried out at 1 GHz by a scanning evanescent microwave probe (SEMP) as a function of A and B concentration in the BST phase (see Figure 2). The dielectric constant and tangent loss decrease in both libraries as A and B concentrations increase. The minimum tangent loss is about 0.05 at 1 GHz for the BST-A libraries, while loss in the BST-B library decreases sharply to below 0.001 (which is the limitation of SEMP) as B concentration increases.

Tunability of the BST-B thin film was measured at 1 MHz by an HP 4280A C–V plotter on an interdigital electrode patterned at the location corresponding to about 22% B. The results for dielectric constant as a function of electrical field are shown in Figure 3. The tunability of BST-22%B is 15% in an electrical field of 4 V/μm, and the tangent loss is again in the noise range of the instrument. A series of ceramic bulk materials with different dielectric constants and tunabilities were further developed based on the BST-B composition. These materials have a dielectric constant ranging from 200 to 1500 and tunability from 20% to 60% in a field of 8 V/μm with tangent loss of the order of 0.001 at 1 GHz. With dielectric tunability comparable to $(BaSr)TiO_3$ and a much lower tangent loss, these materials have great potential for applications in wireless communications, for instance, as tunable filters and beam-steering antennas.

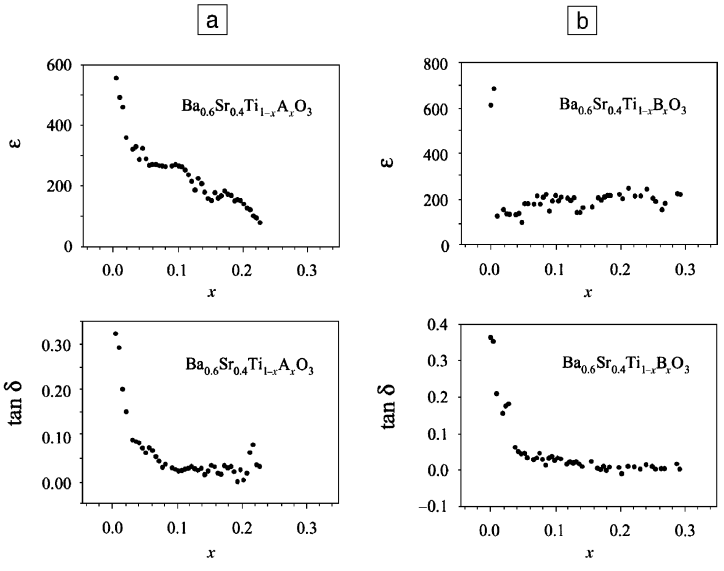

Figure 2. Plots of dielectric constant ε and tangent loss tan δ at 1 GHz as a function of (a) A phase concentration in a BST-A library and (b) B phase concentration in a BST-B library.

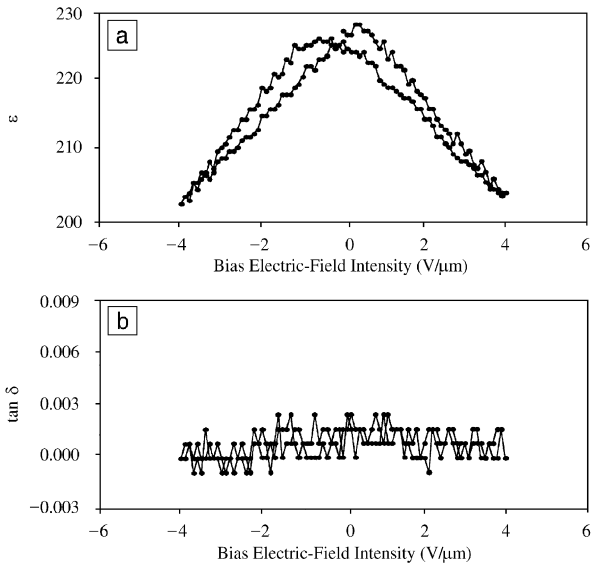

Figure 3. Tunability of (a) dielectric constant ε and (b) tangent loss tan δ for $Ba_{0.6}Sr_{0.4}Ti_{0.78}B_{0.22}O_3$.

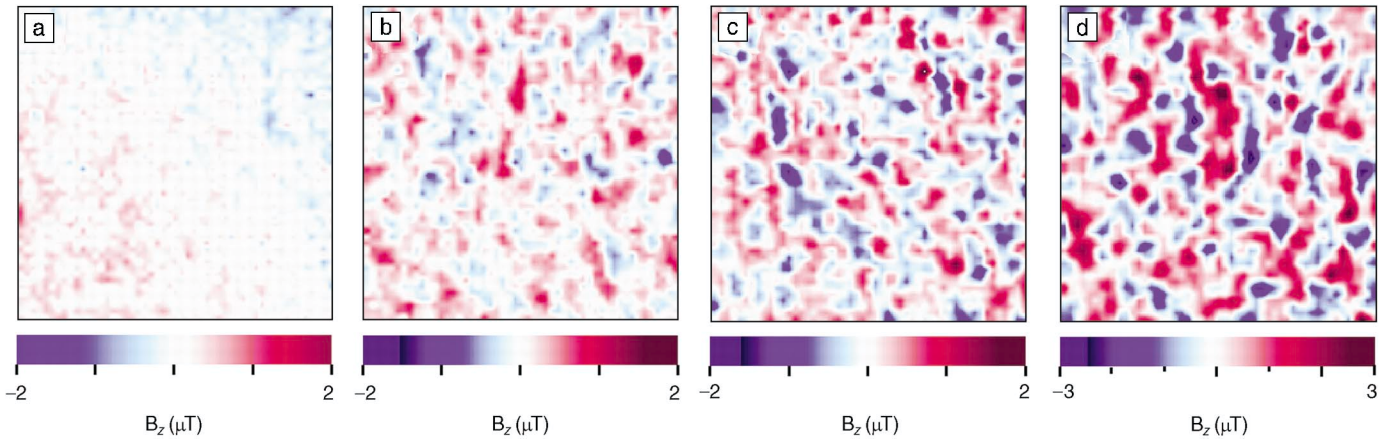

Figure 9. A series of scanning superconducting quantum interference device (SQUID) microscope images (200 μm × 200 μm) taken at 3 K for anatase thin films with different Co contents ($Ti_{1-x}Co_xO_2$) on a combinatorial chip. B_z stands for the magnetic field in the z direction. (a) x = 0, (b) x = 0.02, (c) x = 0.03, and (d) x = 0.06. Magnetic-domain structures were observed in all films, suggesting the presence of long-range ordering. (From Reference 25.)

discussions. We would particularly like to acknowledge the key contributions by our closest co-workers, including H. Chang, T. Chikyow, F. Duewer, T. Fukumura, C. Gao, T. Hasegawa, M. Kawasaki, Y. Matsumoto, T. Ohnishi, 'P.G. Schultz, L.F. Schneemeyer, T. Wei, and X.-D. Xiang.

References

1. X.-D. Xiang, X.-D. Sun, G. Briceño, Y. Lou, K.-A. Wang, H. Chang, W.G. Wallace-Freedman, S.-W. Chen, and P.G. Schultz, *Science* **268** (1995) p. 1738.
2. G. Briceño, H. Chang, X.-D. Sun, P.G. Schultz, and X.-D. Xiang, *Science* **270** (1995) p. 273.
3. H. Chang, C. Gao, I. Takeuchi, Y. Yoo, J. Wang, P.G. Schultz, X.-D. Xiang, R.P. Sharma, M. Downes, and T. Venkatesan, *Appl. Phys. Lett.* **72** (1998) p. 2185.
4. H. Chang, I. Takeuchi, and X.-D. Xiang, *Appl. Phys. Lett.* **74** (1999) p. 1165.
5. I. Takeuchi, H. Chang, C. Gao, P.G. Schultz, X.-D. Xiang, R.P. Sharma, M.J. Downes, and T. Venkatesan, *Appl. Phys. Lett.* **73** (1998) p. 894.
6. I. Takeuchi, K. Chang, R.P. Sharma, L.A. Bendersky, H. Chang, X.-D. Xiang, E.A. Stach, and C.-Y. Song, *J. Appl. Phys.* **90** (2001) p. 2474.
7. H. Koinuma, *Solid State Ionics* **108** (1998) p. 1.
8. H. Koinuma, *Appl. Surface Sci.* (Proc. 1st Japan–U.S. Workshop on Combinatorial Materials Sci. & Tech., 2002) in press.
9. H. Koinuma, T. Koinda, T. Ohnishi, D. Komiyama, M. Lippmaa, and M. Kawasaki, *Appl. Phys. A* **69** (1999) p. S29.
10. M. Kawasaki, K. Takahashi, T. Maeda, R. Tsuchiya, M. Shinohara, O. Ishiyama, T. Yonezawa, M. Yoshimoto, and H. Koinuma, *Science* **266** (1994) p. 1540.
11. T. Ohnishi, D. Komiyama, T. Koida, S. Ohashi, C. Stauter, H. Koinuma, A. Ohtomo, M. Lippmaa, N. Nakagawa, M. Kawasaki, T. Kikuchi, and K. Omote, *Appl. Phys. Lett.* **79** (2001) p. 536.
12. T. Wei, X.-D. Xiang, W.G. Wallace-Freedman, and P.G. Schultz, *Appl. Phys. Lett.* **68** (1996) p. 3506.
13. C. Gao and X.-D. Xiang, *Rev. Sci. Instrum.* **69** (1998) p. 3846.
14. I. Takeuchi, T. Wei, F. Duewer, Y.K. Yoo, X.-D. Xiang, V. Talyansky, S.P. Pai, G.J. Chen, and T. Venkatesan, *Appl. Phys. Lett.* **71** (1997) p. 2026.
15. K.S. Chang, M. Aronova, O. Famodu, I. Takeuchi, S.E. Lofland, J. Hattrick-Simpers, and H. Chang, *Appl. Phys. Lett.* **79** (2001) p. 4411.
16. E.D. Isaacs, M. Kao, G. Aeppli, X.-D. Xiang, X.-D. Sun, P. Schultz, M.A. Marcus, G.S. Cargill, and R. Haushalter, *Appl. Phys. Lett.* **73** (1998) p. 1820.
17. Y.K. Yoo, T. Ohnishi, G. Wang, F.W. Duewer, X.-D. Xiang, Y.-S. Chu, D.C. Mancini, Y.-Q. Li, and R.C. O'Handley, *Intermetallics* **9** (2001) p. 541.
18. K. Omote, T. Kikuchi, J. Harada, M. Kawasaki, A. Ohtomo, M. Ohtani, T. Ohnishi, D. Komiyama, and H. Koinuma, in *Proc. SPIE*, Vol. 3941 (SPIE—The International Society for Optical Engineering, Bellingham, WA, 2000) p. 84.
19. W. Chang, J.S. Horwitz, W.-J. Kim, J.M. Pond, S.W. Kirchoefer, and D.B. Chrisey, in *Ferroelectric Thin Films VII*, edited by R.E. Jones, R.W. Schwartz, S.R. Summerfelt, and I.K. Yoo (Mater. Res. Soc. Symp. Proc. **541**, Warrendale, PA, 1999) p. 699.
20. R.B. van Dover, L.F. Schneemeyer, and R.M. Fleming, *Nature* **392** (1998) p. 162.
21. R.B. van Dover and L.F. Schneemeyer, *IEEE Electron Device Lett.* **19** (1998) p. 329.
22. R.B. van Dover, T. Siegrist, L.F. Schneemeyer, M.L. Green, and L. Manchanda, *Nature* (2002) submitted for publication.
23. G.D. Wilk, R.M. Wallace, and J.M. Anthony, *J. Appl. Phys.* **87** (2000) p. 484.
24. K.J. Hubbard and D.G. Schlom, *J. Mater. Res.* **11** (1996) p. 2757.
25. Y. Matsumoto, M. Murakami, T. Shono, T. Hasegawa, T. Fukumura, M. Kawasaki, P. Ahmet, T. Chikyow, S. Koshihara, and H. Koinuma, *Science* **291** (2001) p. 854.
26. Y. Matsumoto, R. Takahashi, M. Murakami, T. Koida, X.-J. Fan, T. Hasagawa, T. Fukumura, M. Kawasaki, S. Koshihara, and H. Koinuma, *Jpn. J. Appl. Phys., Part 2: Lett.* **40** (2001) p. L1204. □